Sorokin, et al. 2016

Supplemental Materials:

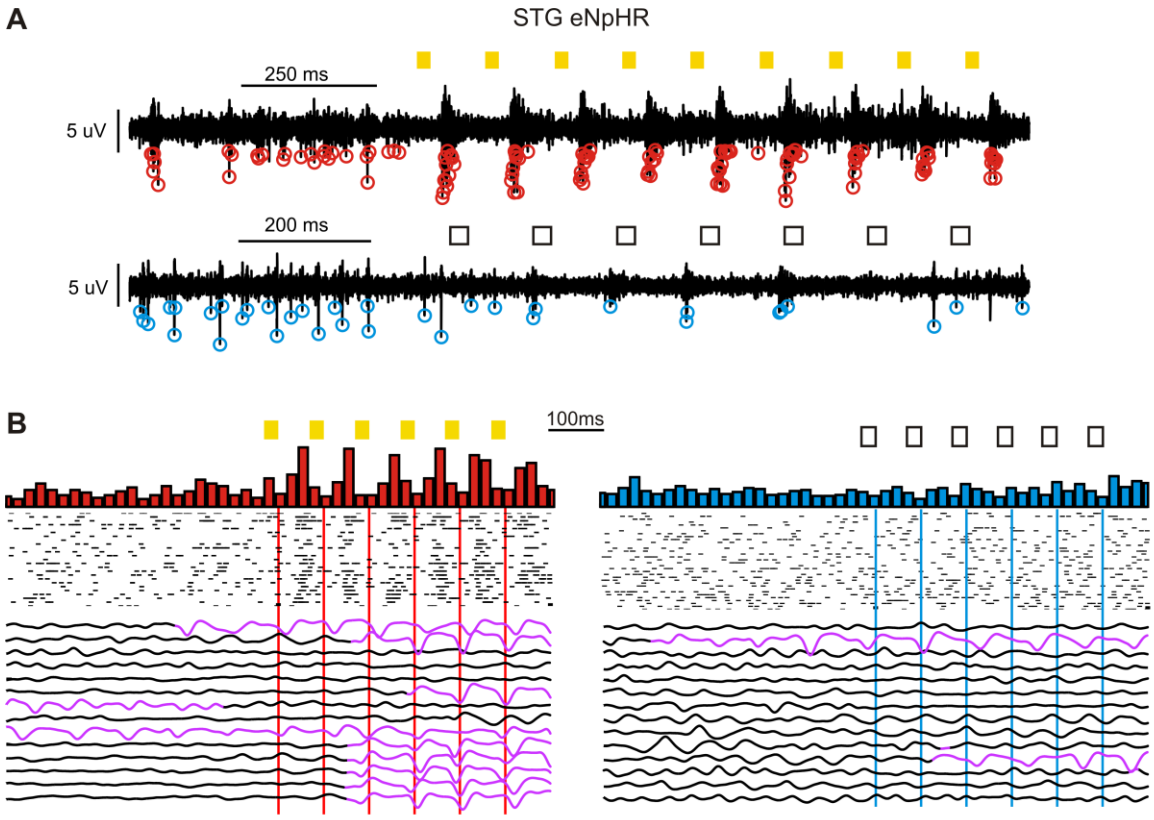

Figure S1; related to Figures 3-5: *Rhythmic activation of eNpHR in TC neurons drives multi-unit (MU) phasic clusters and ECoG SWDs in STG-eNPHR mice*. **(a)** Example trace from an STG-eNPHR mouse showing detected spikes during an 8 Hz laser (*top, red circles*) and sham (*bottom, blue circles*) trial. Yellow/empty bars = 594nm/sham pulses. **(b)** Rasters of MU spikes across laser (*left*) and sham (*right*) trials for another STG-eNPHR mouse during a 12 Hz trial. *Top*: PSTH binned at 40ms; note the coherent increase in MU spiking after each 594nm pulse, which is absent in the sham condition. *Middle*: rasters of MU spikes. *Bottom*: Contralateral ECoG traces with spike-wave discharges (SWDs) highlighted in purple. Note the consistent seizure initiation (after a delay of 3-4 594nm pulses), which is absent in the sham trials. Not all ECoG trials are displayed for clarity. Red/blue vertical lines indicate the end of each laser/sham pulse.

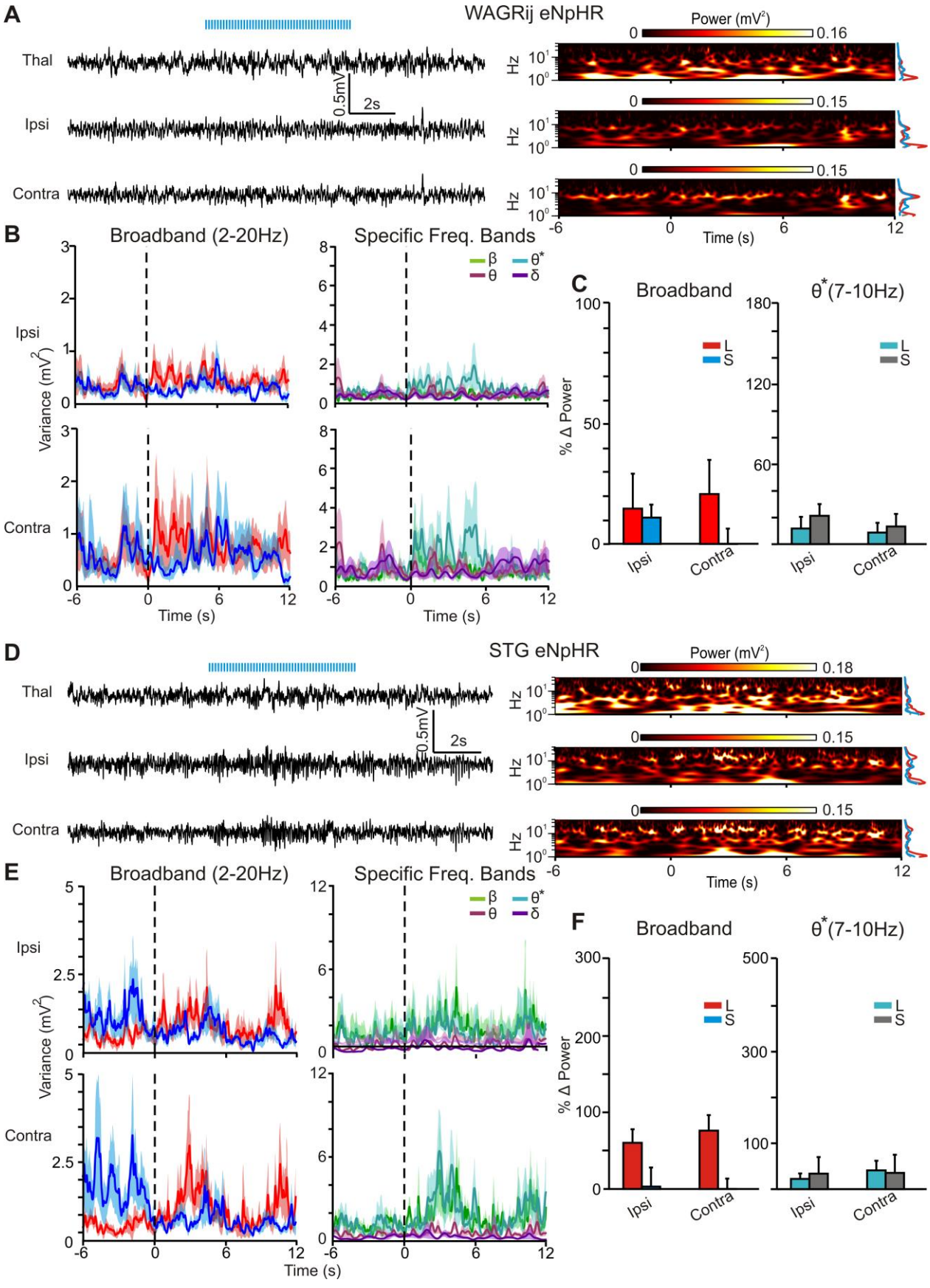
A
WAGRij eNpHR
Power (mV²)
0
0.16
Thal
Ipsi
Contra
0.5mV
2s
Hz
0.15
Time (s)
B
Broadband (2-20Hz)
Specific Freq. Bands
β
θ*
θ
δ
Ipsi
Contra
Variance (mV²)
Time (s)
C
Broadband
θ*(7-10Hz)
% Δ Power
L
S
D
STG eNpHR
0.18
E
F

Figure S2; related to Figures 3-5: *488nm trains do not induce seizures in eNpHR-expressing rodents.* **(a)** *Left*: example trace from a WAG/Rij-eNPHR rat showing thalamic LFP (*top*), ipsilateral ECoG (*middle*), and contralateral ECoG (*bottom*). Blue bars above the traces indicate the 8 Hz pulses of 488nm light, which were delivered to the right VB. *Right*: time-frequency wavelet decomposition of the traces; note the lack of induced power in the 8-16 Hz range across the entire trace. *Right Inset*: Averaged prestim, stim, and poststim power. **(b)** *Left*: trial-averaged broadband (BB 2-20 Hz) variance over time for all laser (red) and sham (blue) trials. *Right*: trial-averaged variance for induced seizures, decomposed into different frequency bands (*ß=10-20Hz; Ø*=7-10 Hz; Ø=4-7 Hz; ∂=2-4 Hz*). Shaded error represents ± s.e.m. **(c)** *Left*: median percent change in BB variance from prestim → stim periods for induced (red) and sham (blue) trials. *Right*: median percent change Ø* variance. Error bars represent ± m.s.e.m. (*Wilcoxon rank sum, 12/15 laser/sham events, 2 trials, 1 animal*). **(d-f)** Same as **a-c,** but for STG-eNPHR (*Wilcoxon rank sum, 7/7 laser/sham events, 2 trials, 2 animals*). See also Video S2.

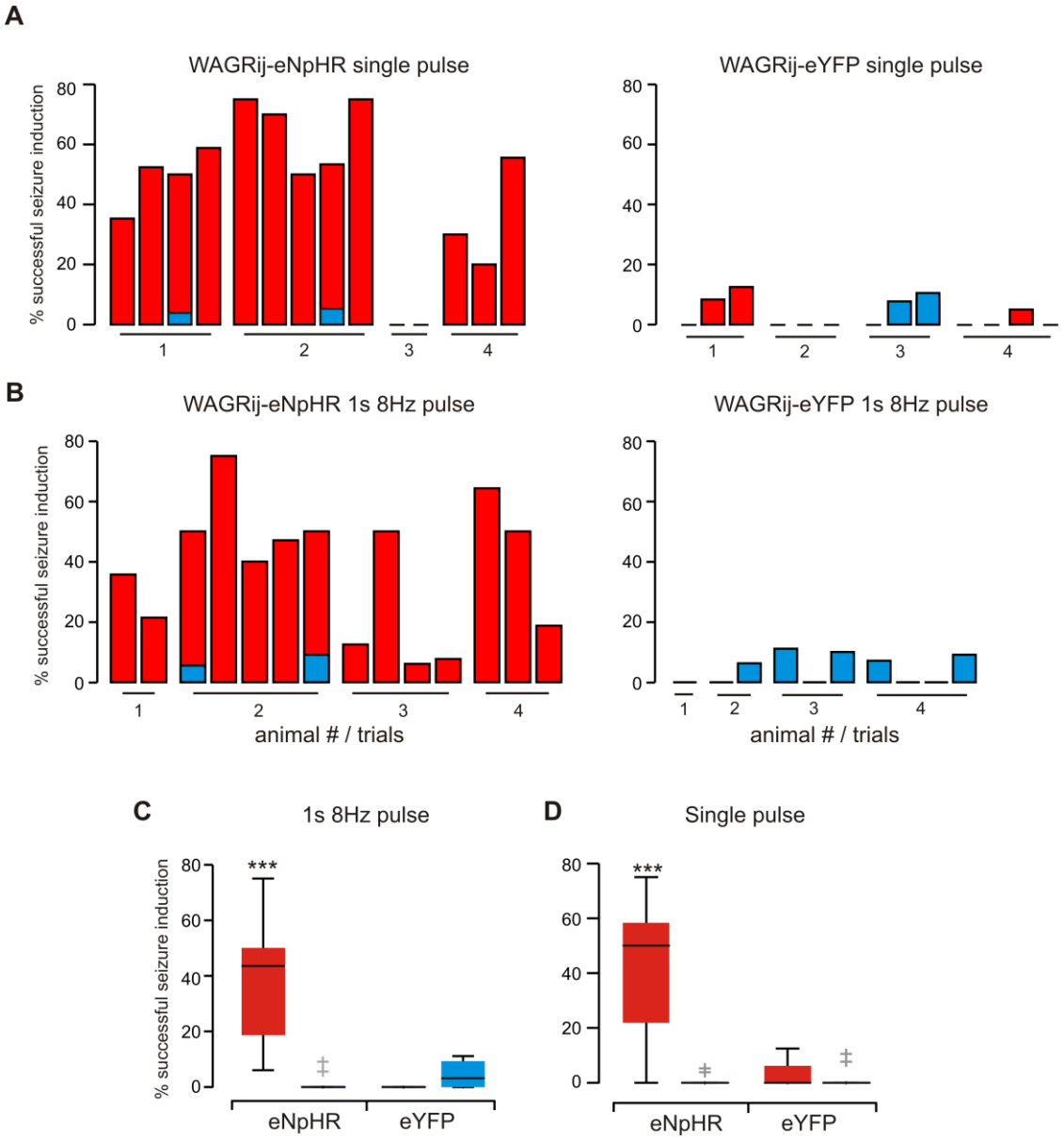

Figure S3; related to Figures 3-5: *Single pulses and short (1s) 8 Hz trains of 594nm light evoke bilateral seizures with much higher probabilities than by chance.* **(a)** Bar graph of the % successfully induced seizures for WAGRij-eNpHR (*left*) and WAGRij-eYFP (*right*) for single-pulse experiments (see Fig. 3), divided by laser (*red*) and sham (*blue*) pulses. Each bar represents one trial, and groups of bars correspond to different animals (labeled 1-4). % success was defined as the number of events (i.e. triggered pulse) that were followed by a seizure within 2 seconds, divided by the total number of events for that trial. Although 594nm light to the right VB does not always induce a seizure, it does so much more often than by chance, as evident by the low probabilities in sham and eYFP conditions. **(b)** Same as **a**, but for short (1s) 8 Hz trains of 594nm light delivered to the right VB (see Fig. 3e-h). **(c)** Box plots of average % success across all trials for eNpHR and eYFP animals for 1s 8 Hz pulses. Only the eNpHR-laser condition resulted in, on average, a significantly higher probability of seizure induction compared to the three other conditions ($p < .001$, *Kruskal-Wallis test; eNpHR: 15 trials, 4 animals; eYFP: 10 trials, 4 animals*). **(d)** Same as **c**, but for single 50ms pulse ($p < .001$, *Kruskal-Wallis test; eNpHR: 15 trials, 4 animals; eYFP: 13 trials, 4 animals).*

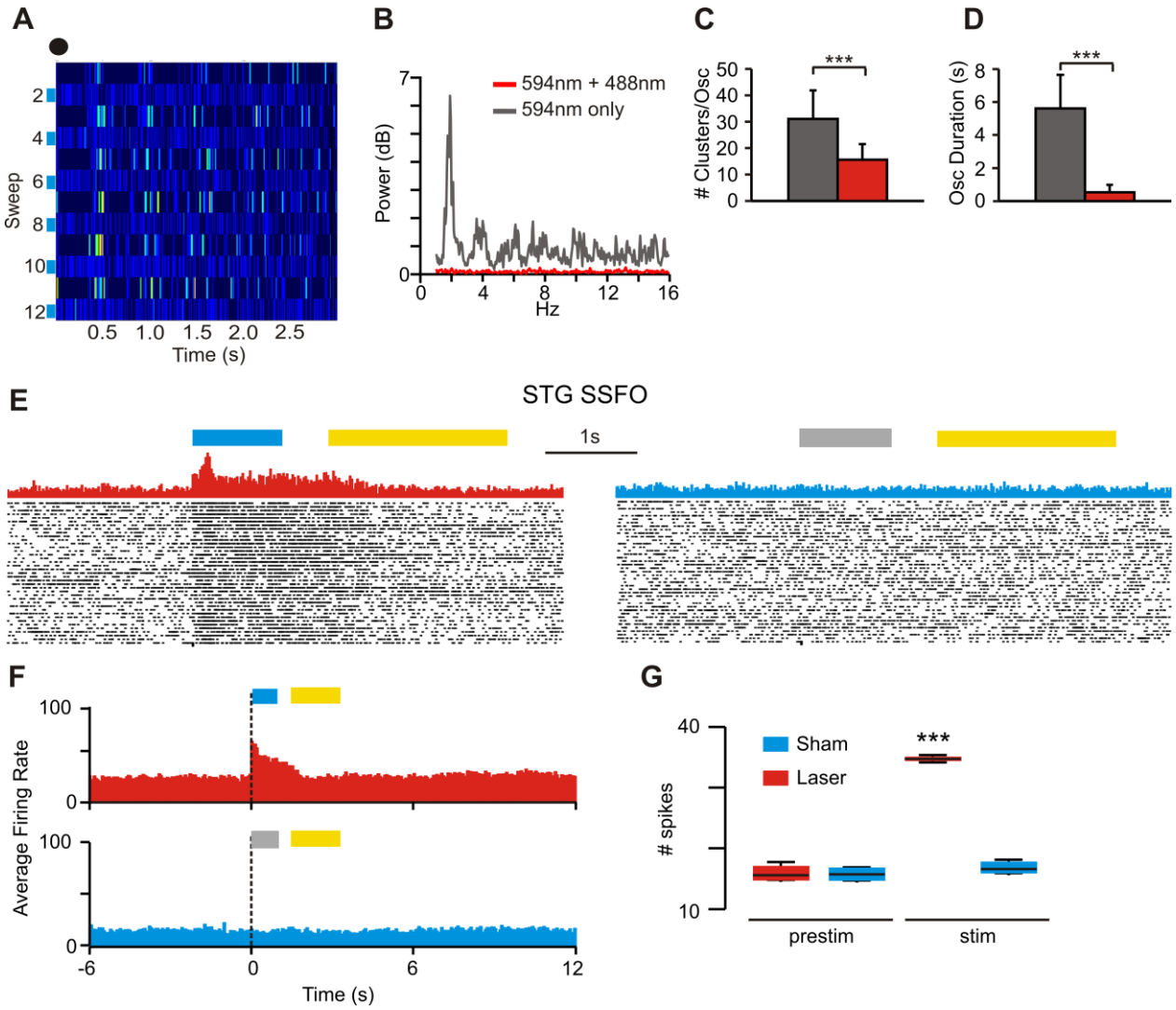

Figure S4; related to Figure 6: *SSFO activation in TC VB neurons robustly eliminates phasic firing and oscillations in thalamic slices and increases tonic firing in STG-SSFO mice.* **(a)** Multi-unit (MU) PSTH of spikes from VB neurons of a WAGRij-SSFO thalamic slice. Y-axis indicates sweep number; x-axis indicates time following the electrical stimulation to the internal capsule (*black dot*). Even-numbered sweeps were primed with 594nm then 488nm light; odd-numbered sweeps were primed only with 594nm light. Coherent periodic bursts emerge only in odd sweeps, while tonic firing appears in even sweeps. **(b)** Average spectrogram across even (*red*) and odd (*gray*) trials from **a**. Odd trials display high 2-3 Hz power, which is characteristic of epileptiform thalamic oscillations *in vitro* and is abolished by SSFO activation. **(c)** Average number of clusters per oscillation across 594nm-only trials (*gray*) and 594nm+488nm trials (*red*). **(d)** Average oscillation duration in seconds. Statistics for **c,d** were based off of $n = 17$ slices, taken from 8 animals. Error bars = $\pm$ s.e.m. *p $\leq$ 0.05 **p $\leq$ 0.01 ***p $\leq$ 0.001, *Students T-test.* **(e)** Rasters of *in vivo* multi-unit (MU) spikes in a STG-SSFO mouse across laser (*left*) and sham (*right*) events during one trial. *Top*: PSTH binned at 40ms; note the increase in firing rate with 488nm light and return to baseline with 594nm light, which are absent in the sham condition (*right*) **(f)** Average PSTH across STG SSFO trials shows a clear increase in firing rate with 488nm light (top) but not sham (bottom). Black vertical lines denote the time of the detected seizure and onset of the light/sham pulse. **(g)** Boxplots of total spike counts 1 second before (*prestim, left*) and during (*stim, right*) the 488nm pulse, averaged across all trials/animals ($p < .001$, *ANOVA, four trials, two animals*).

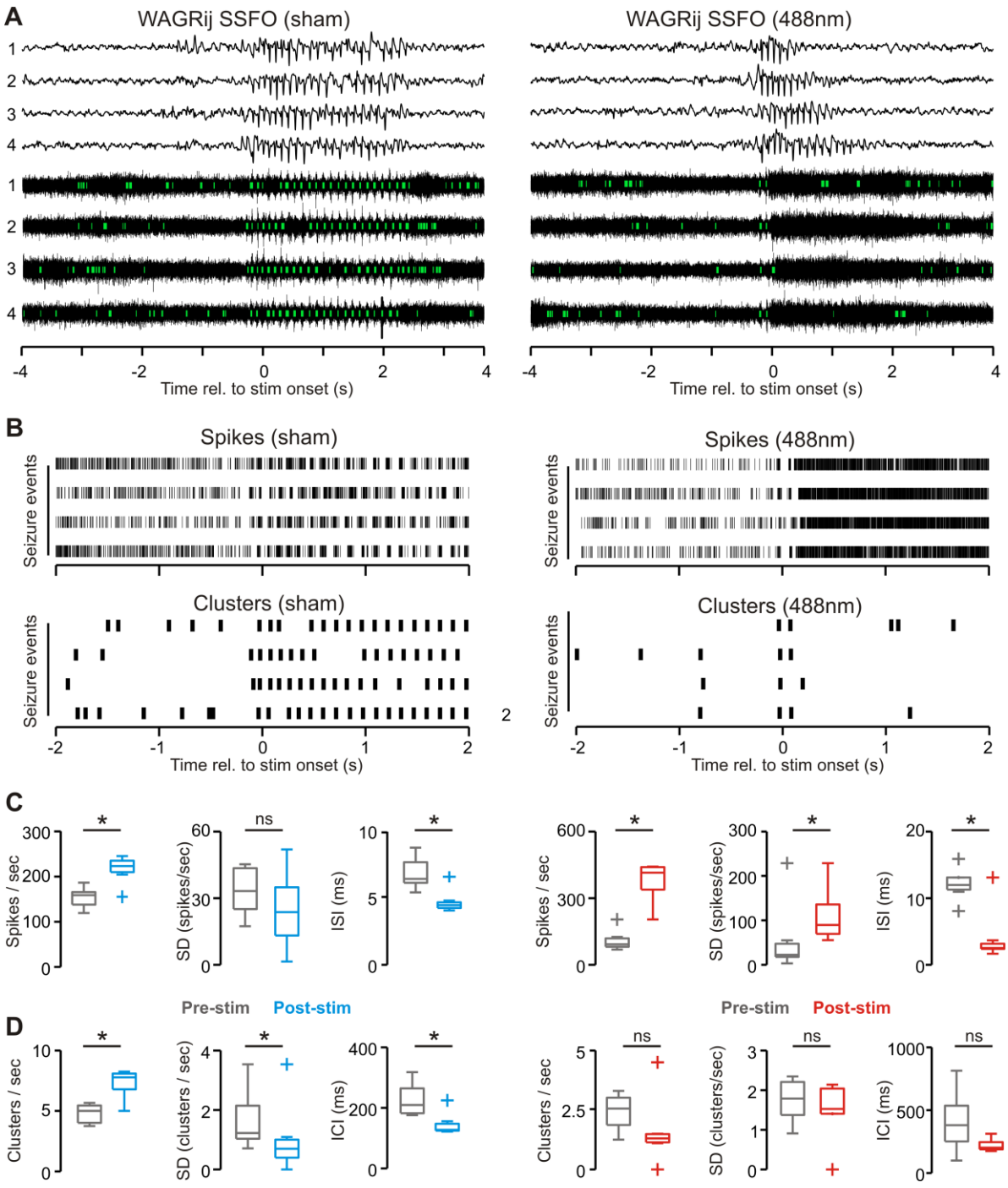

Figure S5; related to Figures 2, 6, 7: *Clustered, high firing-rate output of the VB during spontaneous seizures is transformed into asynchronous tonic firing with SSFO activation.* **(a)** Example ipsilateral ECoG (*top*) and thalamic multi-unit activity (*bottom*) with detected SPCs (*green*) from four spontaneous seizures in a WAGRij-SSFO rat without SSFO activation (*left*), and with SSFO activation (*right*) via 488nm light delivered to the VB; notice the immediate abolishment of bursts with 488nm light. **(b)** Rasters of spikes (*top*) and population spike clusters (*bottom*) without SSFO activation (*left*) and with activation (*right*) from the same animal/trial as in **(a)**. **(c)** The spike rate (*left*), intra-trial s.d. of the spike rate (*middle*), and the inter-spike interval (*right*) averaged over 2-second windows prior to the seizure onset (*gray*) and following the seizure onset (*blue, red*) across all trials from one WAGRij-SSFO animal. The left three box plots (*blue*) correspond to sham pulses, while the right three (*red*) correspond to SSFO activation via 488nm light. **(d)** Same as **(c)** but for cluster rate, intra-trial s.d. of cluster rate, and inter-cluster interval; note that cluster rates are relatively low following SSFO activation compared to sham. (*n = seven trials, one animal; Wilcoxon Signed-Ranks test; * $p \leq 0.05$)*

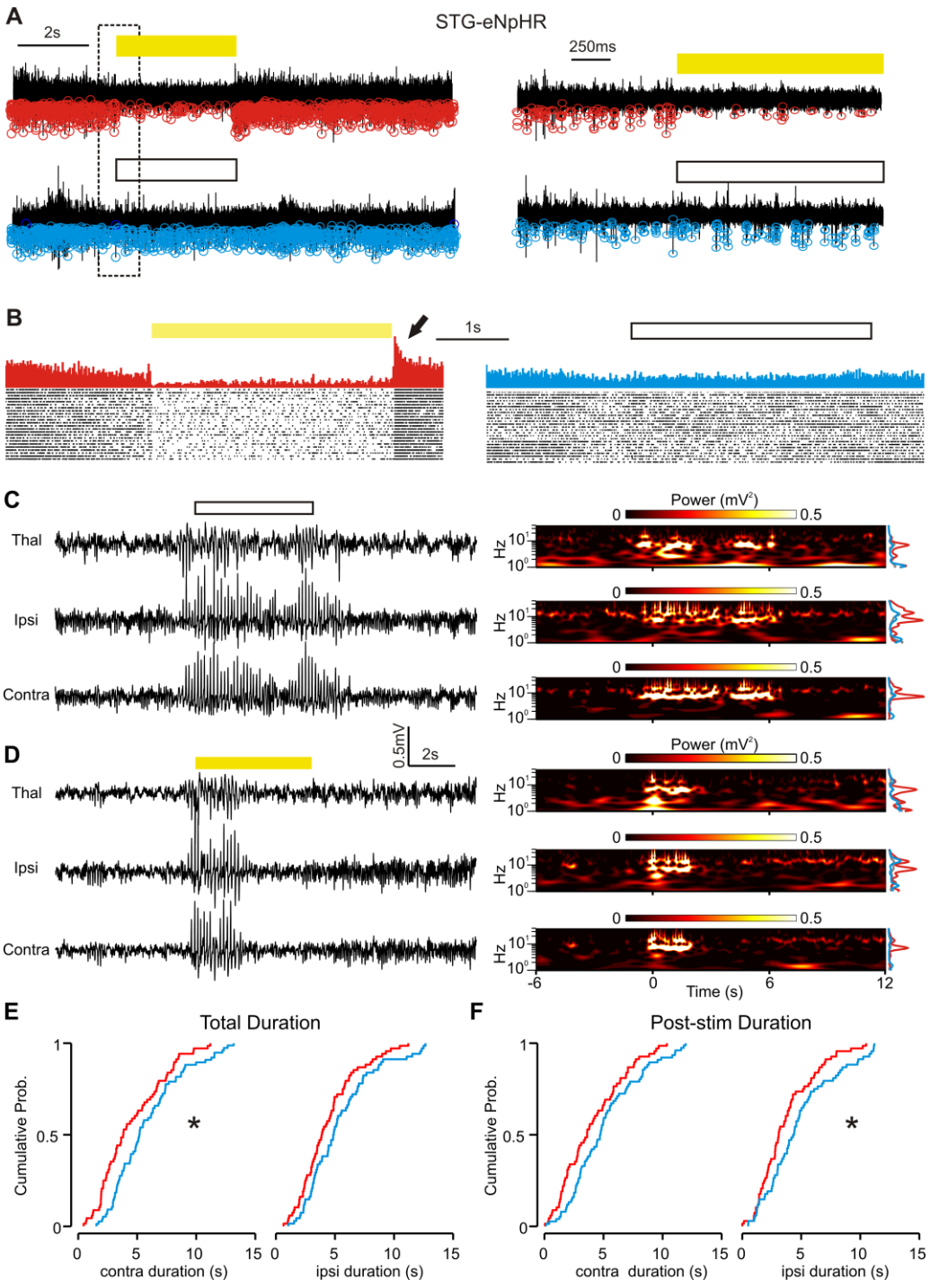

Figure S6, related to Figure 7: *Real-time unilateral inhibition of VB via eNpHR bilaterally shortens absence seizures in STG mice.* **(a)** Multi-unit activity with spikes overlaid (*red, blue circles*) from an STG-eNpHR mouse demonstrating the inhibitory effects of eNpHR on VB firing with 594nm light (*top*) vs. sham (*bottom*). *Right inset:* zoom of the boxed-region on the left. **(b)** Spike rasters (bottom) and average PSTH (*top*) across all real-time detected seizures in one trial/animal for laser (*left*) and sham (*right*) pulses. There is strong post-inhibitory rebound activity evident in the post-laser PSTH (*arrow*). **(c)** Thalamic LFP and ipsilateral/contralateral ECoG traces (*left*) and their corresponding wavelet power spectra (*right*) during a spontaneous seizure with a sham pulse. Note the strong ~8Hz band in the power spectra that persists throughout the seizure. **(d)** Same as **c,** but with 594nm light delivered to the right VB. **(e)** Cumulative distributions of total contralateral and ipsilateral (*left, right*) seizure lengths across all STG animals, separated by laser (*red*) and sham (*blue*) pulses. **(f)** same as **e**, but for post-stimulus seizure durations. (**e,f:** *68/76 (left) and 68/68 (right) laser/sham seizures, four trials, three animals; Kolmogorov-Smirnov test, *p ≤ 0.025).*

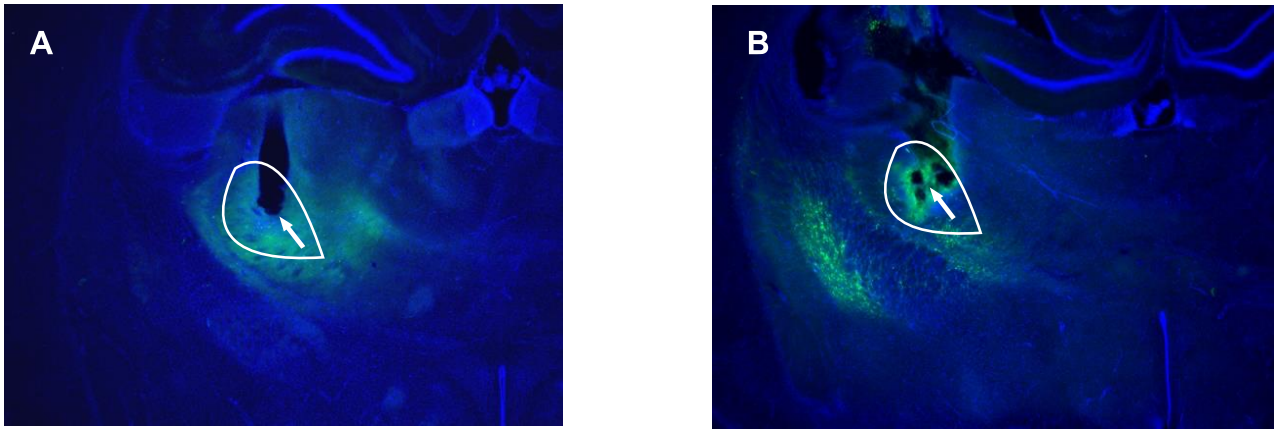

Figure S7, related to experimental procedures: *Histology of viral injections and optrode implants.* Representative histological images of two different WAGRij rats used for *in vivo* recordings. Blue = dapi, green = eYFP-tagged opsin. White ovals demarcate the thalamic ventrobasal (VB) complex. Note that in **b** thalamocortical fibers expressing eYFP are seen projecting through the striatum.

594nm	Single pulse	3Hz	8Hz	8Hz (1s)	12Hz	20Hz
WAGRij eNpHR						
n	15 trials (4 animals)	5 trials (4 animals)	23 trials (5 animals)	7 trials (4 animals)	11 trials (5 animals)	14 trials (5 animals)
BB (power)	137.58 ± 27.46	144 ± 102.44	490.08 ± 57.98	173.88 ± 42.82	267.90 ± 70.44	204.26 ± 56.02
ß (power)	158.93 ± 39.54	232.30 ±108.79	844.04 ± 119.02	318.11 ± 85.66	598.19 ± 168.95	405.70 ± 105.18
Ø (power)*	190.68 ± 48.84	447.70 ± 190.67	975.09 ± 137.14	335.98 ± 93.35	186.85 ± 61.17	318.53 ± 105.65
Ø (power)	112.16 ± 27.2	528.28 ± 193.82	235.56 ± 38.92	84.58 ± 16.33	219.13 ± 66.17	102.04 ± 32.09
∂ (power)	78.30 ± 21.32	330.11 ± 146.44	90.69 ± 14.66	29.83 ± 9.28	31.98 ± 17.58	40.56 ± 10.58
WAGRij eYFP						
n	6 trials (4 animals)	n/a	11 trials (5 animals)	4 trials (4 animals)	9 trials (4 animals)	7 trials (4 animals)
BB (power)	9.06 ± 7.77	n/a	-2.18 ± 2.28	4.71 ± 5.36	22.04 ± 11.14	27.62 ± 12.10
ß (power)	7.08 ± 3.92	n/a	-1.75 ± 4.64	11.81 ± 2.44	24.74 ± 21.50	33.46 ± 12.59
Ø (power)*	4.02 ± 4.00	n/a	2.22 ± 5.15	5.21 ± 2.82	34.77 ± 23.53	26.45 ± 13.54
Ø (power)	23.25 ± 6.66	n/a	14.47 ± 6.85	13.33 ± 7.53	25.87 ± 18.16	25.92 ± 7.31
∂ (power)	22.71 ± 8.70	n/a	9.89 ± 4.49	12.04 ± 5.46	21.56 ± 11.21	24.82 ± 16.59
STG eNpHR						
n	n/a	5 trials (3 animals)	7 trials (3 animals)	n/a	5 trials (3 animals)	5 trials (3 animals)
BB (power)	n/a	47.34 ± 8.21	267.81 ± 10.35	n/a	99.11 ± 22.60	118.49 ± 13.62
ß (power)	n/a	80.79 ± 12.74	243.95 ± 9.72	n/a	118.78 ± 24.47	185.91 ± 23.43
Ø (power)*	n/a	59.73 ± 9.59	361.96 ± 15.48	n/a	131.68 ± 24.73	100.27 ± 12.46
Ø (power)	n/a	32.31 ± 6.45	91.77 ± 5.20	n/a	92.36 ± 17.46	35.66 ± 6.75
∂ (power)	n/a	17.66 ± 4.60	29.17 ± 2.63	n/a	-1.9 ± 6.63	-13.98 ± 3.75
Sham	**Single pulse**	**3Hz**	**8Hz**	**8Hz (1s)**	**12Hz**	**20Hz**
WAGRij eNpHR						
n	15 trials (4 animals)	5 trials (4 animals)	24 trials (5 animals)	7 trials (4 animals)	11 trials (5 animals)	14 trials (5 animals)
BB (power)	38.9 ± 26.6	-26.7 ± 16.63	19.36 ± 9.10	10.21 ± 11.26	17.43 ± 11.14	9.58 ± 3.13
ß (power)	9.12 ± 4.39	-27.47 ± 9.41	34.53 ± 13.72	10.93 ± 10.46	19.64 ± 12.76	11.47 ± 3.48
Ø (power)*	9.16 ± 5.64	-3.89 + 13.36	13.94 ± 10.25	10.73 ± 10.04	8.56 ± 3.92	15.33 ± 4.90
Ø (power)	87.92 ± 60.28	-7.54 ± 18	23.00 ± 7.50	18.31 ± 11.82	11.82 ± 11.98	12.87 ± 5.11
∂ (power)	30.16 ± 7.90	-20.06 ± 14.29	23.13 ± 7.24	32.10 ± 13.81	23.99 ± 16.02	14.84 ± 5.63
WAGRij eYFP						
n	6 trials (4 animals)	n/a	10 trials (5 animals)	4 trials (4 animals)	9 trials (4 animals)	7 trials (4 animals)
BB (power)	5.26 ± 3.99	n/a	0.14 ± 2.81	57.21 ± 32.08	8.06 ± 4.74	20.56 ± 9.78

ß (power)	4.06 ± 6.89	n/a	9.54 ± 4.49	62.11 ± 35.15	11.56 ± 7.44	26.85 ± 8.06
Ø (power)*	6.37 ± 2.60	n/a	-0.73 ± 3.21	64.28 ± 42.80	13.54 ± 4.34	19.83 ± 9.32
Ø (power)	10.78 ± 3.67	n/a	9.96 ± 4.98	65.86 ± 27.51	-5.98 ± 6.86	23.24 ± 19.69
∂ (power)	14.19 ± 10.73	n/a	9.70 ± 4.18	57.47 ± 19.82	17.50 ± 8.74	19.16 ± 14.16
STG eNpHR						
n	n/a	5 trials (3 animals)	7 trials (3 animals)	n/a	5 trials (3 animals)	5 trials (3 animals)
BB (power)	n/a	1.28 ± 4.14	3.86 ± 2.35	n/a	-4.67 ± 3.11	-4.93 ± 4.91
ß (power)	n/a	-1.43 ± 5.29	-0.84 ± 3.37	n/a	-17.68 ± 6.01	-4.22 ± 5.56
Ø (power)*	n/a	0.11 ± 5.80	7.55 ± 3.61	n/a	-16.92 ± 5.09	-5.45 ± 6.42
Ø (power)	n/a	18.53 ± 5.84	-0.19 ± 2.65	n/a	-13.33 ± 6.40	-3.16 ± 5.54
∂ (power)	n/a	12.88 ± 3.98	-4.87 ± 2.38	n/a	-13.22 ± 4.69	0.3 ± 5.36

Table S1; related to Figures 3-5, S1: *Activation of eNpHR in TC neurons in VB drives contralateral thalamocortical oscillations in STG-eNpHR and WAGRij-eNpHR, but not WAGRij-eYFP.* C*olumns*: Seizure power of contralateral ECoG channel decomposed into different frequency bands (BB=2-20Hz; ß=10-20Hz; Ø*=7-10 Hz; Ø=4-7 Hz; ∂=2-4 Hz) vs. different pulse train frequencies of 594nm light or sham pulses. Under each condition (STG-eNpHR, WAGRij-eNpHR, WAGRij-eYFP), the first row shows the total number trials in each recording condition and the number of animals. Values listed are medians ± m.s.e.m. (see *statistics* in supplemental experimental procedures) of the percent change in band variance between baseline (pre-stim) and stim periods.

For this table and the following table we report raw values for each recording condition for completeness, but for clarity do not report indicators of statistical significance, as there are multiple dimensions of statistical comparisons across recording conditions.

488nm	n	mean length (s)	med Length (s)	Sham	n	mean length (s)	med Length (s)
STG SSFO				**STG SSFO**			
ipsilateral	4 trials (3 animals)	1.54 ± 0.13	1.49 ± 0.09	*ipsilateral*	4 trials (3 animals)	2.33 ± 0.17	2.14 ± 0.13
contralateral	4 trials (3 animals)	2.85 + 0.14	2.77 ± 0.11	*contralateral*	4 trials (3 animals)	3.55 ± 0.15	3.37 ± 0.12
WAGRij SSFO				**WAGRij SSFO**			
ipsilateral	13 trials (3 animals)	1.97 ± 0.30	1.54 ± 0.28	*ipsilateral*	13 trials (3 animals)	3.36 ± 0.10	3.35 ± 0.08
contralateral	10 trials (3 animals)	2.15 ± 0.35	2.05 ± 0.26	*contralateral*	10 trials (3 animals)	3.15 ± 0.27	3.05 ± 0.211
WAGRij YFP				**WAGRij YFP**			
ipsilateral	13 trials (3 animals)	4.95 ± 0.56	5.00 ± 0.39	*ipsilateral*	12 trials (3 animals)	5.08 ± 0.61	5.45 ± 0.49
contralateral	13 trials (3 animals)	4.93 ± 0.58	5.07 ± 0.42	*contralateral*	12 trials (3 animals)	4.56 ± 0.50	4.63 ± 0.38

Table S2; related to Figures 6, 7, S4: *Activation of SSFO in TC VB neurons interrupts absence seizures in STG and WAGRij-SSFO, but not eYFP. Left:* Seizure lengths for STG-SSFO (*top 3 rows*), WAGRij-SSFO (*middle 3 rows*), and WAGRij-eYFP (*bottom 3 rows*) for both ipsilateral and contralateral cortices during SSFO closed-loop seizure interruption with 488nm light. The first column ("n") shows the number of trials and animals used for our analyses in each group. The second and third columns show the mean and median seizure length across all recordings/trials per group, ± s.e.m. or m.s.e.m., respectively. *Right:* same as left, but for all sham pulses.

Supplemental Videos

Video S1, related to Figure 3: *Optogenetically-induced and spontaneous absence seizures*
The Video shows a representative recording of interictal and ictal activities from cortical ECoGs (top, red traces), thalamic LFPs (middle, black traces) from 4 thalamic channels and a yellow (594nm) laser channel (bottom trace) in a behaving STG mouse. The locations of thalamic electrodes 1-4 and of EcoG electrodes are similar to (23). At 7s: a train of 594nm yellow light pulses induces spike-and-wave discharges (SWDs) in both ipsilateral and contralateral EcoGs and that these SWDs outlast the train duration in both thalamic LFP and EcoG. Note that SWDs are associated with a behavioral arrest typical of absence seizures. At 25s: a spontaneous SWD seizure occurs, characterized by a behavioral arrest and by cortical and thalamic oscillations similar to those induced with light.

Video S2, related to Figure 3, S2: *Optogenetically-induced seizures are wavelength specific*
A train of 8 Hz blue (488nm) light (pink stim channel, bottom), which is insufficient at activating eNpHR, does not induce an SWD in a behaving STG mouse (same mouse as in Video S1). Although light artifacts are clearly observed in thalamic channels (especially T3-4), there is no effect on thalamocortical oscillations or behavior.

Video S3, related to Figure 4: *3 Hz 594nm light recruits 8 Hz thalamocortical network activity*
Representative recording of thalamic LFP (T1-4), and contralateral/ipsilateral cortical ECoG (CA, IA) during a 3 Hz train of 594nm pulses (25ms duty cycle; note large light artifacts in thalamic channels). After a few pulses 8 Hz oscillations begin to emerge in thalamic and cortical signals. Both the 8 Hz spike-and-wave discharges (SWDs) and associated behavioral arrest outlast the pulse train.

Video S4, related to Figure 7: *Brief 488nm light (but not sham) bilaterally aborts absence seizures in STG and WAGRij*
This Video shows the representative effects of 488nm light of detected absence seizures in a STG mouse and WAGRij rat expressing SSFO in the right VB. For the STG, a spontaneous absence seizure begins at 10s and is detected at 11s without light delivery (sham pulse…small negative deflection in bottom *stim* channel). There is no effect of the subsequent yellow pulse (larger deflection at 16s) on either cortical (CA, IA) or thalamic (T1-4) channels. The seizure persists and is re-detected at 18s, again without light delivery. Soon after, another seizure begins (25s), is detected within 3 SWD cycles in the cortex, and is immediately aborted with 488nm light (large deflection in the *stim* channel; note thalamic light artifacts).

For the WAGRij, a seizure begins and is detected at 45s, and 488nm light is delivered to the right VB, which immediately aborts the seizure and promotes and arousal response in the rat. Note the large thalamic deflections at 46s and 48s are due to light artifacts from 594nm light, which is used to shut off SSFO.

Video S5, related to Figure 7: *488nm, but not 594nm, light promotes arousal in a sleeping WAGRij-SSFO rat*
Here we show that 594nm light alone does not change the behavioral state of a WAGRij-SSFO rat, arguing that arousal observed with 488nm light is due to SSFO activation and not the light per se. Large delta waves (1-4 Hz) evident in all channels are unperturbed with yellow light (starting at 5 s), and the animal remains in a sleep state long after the yellow light pulse terminates. This is in stark contrast with the 488nm pulse to the same rat (23s), which immediately abolishes slow delta waves, desynchronizes the ECoG and thalamic LFP, and awakens the animal.

Supplemental Experimental Procedures

Statistical and experimental design. We used non-parametric statistics for data that did not pass normality tests. For bar charts, we displayed variance for means as standard error of measurement (s.e.m.) and analogously for medians as median absolute deviation / √n (m.s.e.m.). For box plots, we displayed variances as means (middle bar), 25-75% range (boxes), and 5-95% range (whiskers). Degrees of freedom were defined as $n - 1$ for T-test, Wilcoxon Rank Sum, and Wilcoxon Signed-Rank, and $(c-1) / (n-c)$ for ANOVA and Kruskal-Wallis, where c is number of groups and n is total number of samples used. Sample sizes were chosen using a power analysis prior to experiments. We used multiple animals of both genders and multiple trials for all experiments except for the statistics shown in Supplementary Fig. 5, which uses multiple trials from one WAGRij SSFO animal, as we were unable to isolate well-resolved spikes in the other SSFO rats. We assessed significance by performing one-way ANOVA or the Kruskal-Wallis test for multi-group comparisons, and the Students T-test, Wilcoxon Rank-Sum, or Wilcoxon Signed-Rank tests for individual comparisons. We performed statistical analysis with MATLAB 2013a (MATLAB 8.1, The MathWorks Inc. Natick, MA, 2013). Due to the nature of the experiments, we were not blinded during recordings, as we were able to observe light artifacts in thalamic LFP as well as changes in multi-unit firing rates and ECoG oscillations with light delivery vs. sham. We corrected for multiple comparisons using the Turkey-Kramer (ANOVA), Dunn-Sidak (Kruskal-Wallis), or Bonferroni corrections.

Optrode design and implantation. Optrodes were manufactured in house from readily available materials. First, a 200um-core fiber optic (Thorlabs, Newton, NJ) was cleaved with a ruby scribe to 1mm in length, and secured to a 2x5-pin male-female mill-max (Mill-Max Manufactoring Co., Oyster Bay, NY) with epoxy, after we had initially removed the mill-max pins. Each fiber optic segment was tested to ensure light was not distorted due to the cleaving process. The fiber was situated to run parallel to the mill-max pins slots. After the epoxy had secured, we slipped a small (400um) piece of polyimide tubing (0.015'' diameter) over the fiber optic, and then placed four individual tungsten wires through the tubing. We aligned the recording-ends of the tungsten wires to sit ~250um apart from one another in a linear arrangement, and secured the wire/fiber bundle by placing a small drop of cyanoacrylate glue at the base of the polyimide tubing. We then slipped the other end of each tungsten wire through an empty pinhole in the mill-max, and established an electrical connection by re-inserting the pins, which strips the insulating coating. For ECoG electrodes, we hand-soldered small (.0047'' thread, 1/8'' length) screws to ½'' segments of insulated silver wire, and secured the wires to the optrode by slipping them through the other pinholes in the mill-max and re-inserting the pins as before.

Implants were carried out in a stereotaxic frame. Animals were anesthetized with isofluran and secured with ear bars while resting on top of a small heating pad to maintain body temperature. Prior to surgery, animals were injected with the analgesic carprofen at 2mg/kg. Small bur holes were drilled using a hand-held dremel, and were located above the right VB, bilaterally over the anterior somatosensory cortex and posterior somatosensory cortex, and cerebellum. Optrodes were secured to our stereotaxic frame and implanted by first screwing the ECoG electrodes into the bur holes, then lowering the fiber/tungsten bundle into the thalamus. We used dental cement to secure the optrode, and liberally applied topical lidocaine and antiseptic ointment to the skin surrounding the implant. Animals were monitored for 1 week as they recovered, and were given carprofen tablets to reduce inflammation and pain.

***In vivo* recordings.** All recorded signals (ECoG/LFP/MU) were referenced to the ECoG electrode placed over the cerebellum. ECoG/LFP data were bandpass filtered between 1 and 100 Hz and semi-automatically cleaned of most movement artifacts using wavelet-enhanced independent components analysis, while MU signals were bandpass filtered between 300 and 6000 Hz. Filtered data were saved to disk, and analyzed offline using MATLAB 2013a. Because MU signals degrade over time, likely due to a building glial scar and/or drifting cells, we performed our recordings as soon as possible after implantation (typically following 1 week, or as soon as animals had fully recovered).

Implant/virus targeting confirmation. Following *in vivo* recordings, we validated our targeting for both the viral injection and optrode implantation. Animals were anesthetized and perfused with ice-cold 4% paraformaldehyde (PFA). Implants were then detached from the skull by pulling upward orthogonally, and brains were removed and placed in 4% PFA overnight, followed by 30% sucrose for 24 hours. We then embedded each brain into 2% agarose and took 40-60um coronal sections using a VT1000 vibratome (Leica Biosystems, Wetzlar, Germany). Slices were stained with dapi, mounted and coverslipped, and imaged using an upright BZ-x700 fluorescent microscope (Keyence Co., Osaka, Japan); see Fig. S7 for examples.

False-positive event rejection. We performed thorough seizure validation for each channel separately to ensure noise, artifacts, and other confounding factors were not included in our analyses. Additionally, for induction experiments seizures were rejected if they had initiated spontaneously prior to the stimulus onset, while for interruption experiments seizures were rejected if they had begun to dwindle or if the seizure had been ongoing for greater than 2s prior to stimulus onset, as

well as if stimulus was triggered off of a false positive. False positives were defined as short, high amplitude events lasting less than 200ms, or events with maximum relative power in low frequencies (< 4 Hz) as real SWD have little slow-wave power. In this way, our rejection criteria were extremely *conservative*. No statistics were run on LFP thalamic channels during stimulus periods due to large light artifacts. Because each channel had variable signal quality, we rejected unequal numbers of seizures for different channels, but recorded the indexes of each seizure for proper *post hoc* analysis. To validate our manual rejection in an unbiased manner, we developed an automatic rejection algorithm based on the above criteria, which produced nearly equivalent results to our manual rejection.

Repeatability of experiments. We were able to repeat all reported experiments in multiple animals, in two species, over multiple weeks. Representative *in vivo* ECoG and MU traces for both induction and interruption (closed-loop) experiments exemplify the most common results; there were instances for both sets of experiments in which light pulses did not effectively alter ECoG or the behavior, however these were outweighed by successful results which occurred with a much higher probability than by chance alone (see Fig. S3).